KURENAI 紅

Kyoto University Research Information Repository

KYOTO UNIVERSITY

Title	Spin dependent inelastic collisions between metastable state two-electron atoms and ground state alkali-atoms
Author(s)	Schäfer, Florian; Konishi, Hideki; Bouscal, Adrien; Yagami, Tomoya; Takahashi, Yoshiro
Citation	New Journal of Physics (2017), 19(October 2017)
Issue Date	2017-11-01
URL	http://hdl.handle.net/2433/244802
Right	Original content from this work may be used under the terms of the Creative Commons Attribution 3.0 licence. Any further distribution of this work must maintain attribution to the author(s) and the title of the work, journal citation and DOI.; © 2017 IOP Publishing Ltd and Deutsche Physikalische Gesellschaft
Type	Conference Paper
Textversion	publisher

Kyoto University

New Journal of Physics

The open access journal at the forefront of physics

CrossMark

PAPER

Spin dependent inelastic collisions between metastable state two-electron atoms and ground state alkali-atoms

Florian Schäfer[1] , Hideki Konishi[1], Adrien Bouscal[1,2], Tomoya Yagami[1] and Yoshiro Takahashi[1]

[1]   Department of Physics, Graduate School of Science, Kyoto University, Kyoto 606-8502, Japan
[2]   Department of Physics, École Normale Supérieure, 24 rue Lhomond, F-75231 Paris Cedex 05, France

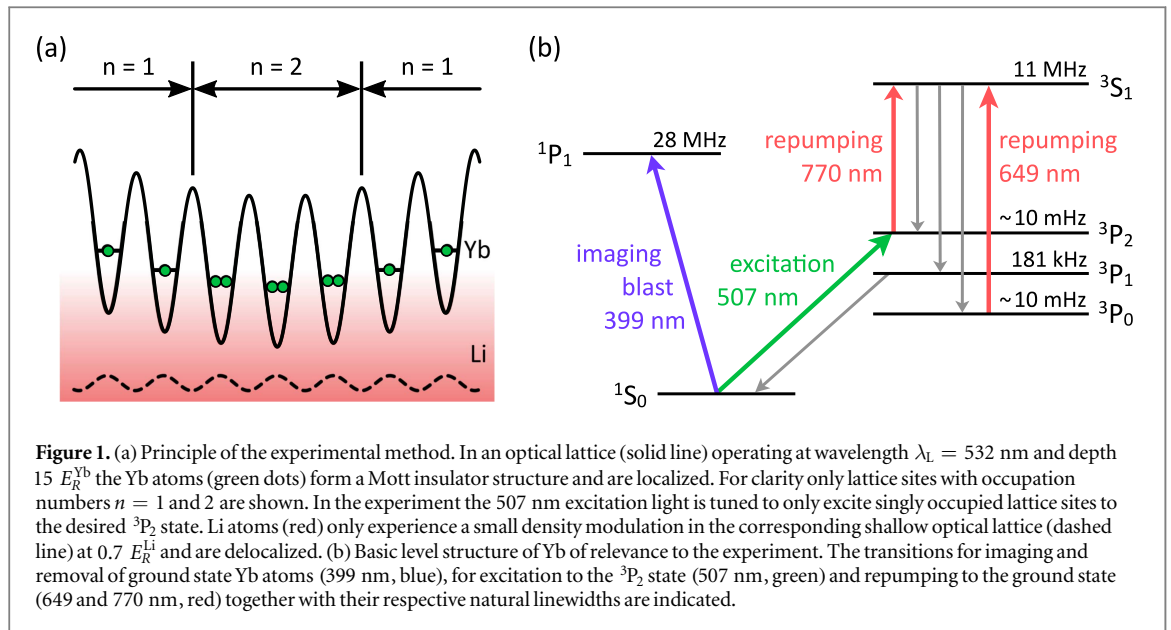E-mail: schaefer@scphys.kyoto-u.ac.jp

Abstract

Experimentally the spin dependence of inelastic collisions between ytterbium (Yb) in the metastable $^3P_2$ state and lithium (Li) in the $^2S_{1/2}$ ground state manifold is investigated at low magnetic fields. Using selective excitation all magnetic sublevels m_J of $^{174}Yb\,(^3P_2)$ are accessed and four of the six lowest lying magnetic sublevels of ^6Li are prepared by optical pumping. On the one hand, m_J-independence of collisions involving $Li\,(F = 1/2)$ atoms is found. A systematic m_J-dependence in collisions with $Li\,(F = 3/2)$ atoms, in particular suppressed losses for stretched collisional states, is observed on the other hand. Further, m_J-changing processes are found to be of minor relevance. The span of observed inelastic collision rates is between 1×10^{-11} and 40×10^{-11} cm^3 s^{-1}, and a possible origin of the observed behavior is discussed.

1. Introduction

Experiments with ultracold atomic gases in combination with optical lattices are a cornerstone in the investigation of quantum matter with, among others, applications in quantum simulation and many-body physics [1]. While these single-component quantum gas systems are essentially defect-free, the investigation of multi-component quantum gases allows for a quantum simulation of phenomena requiring impurities [2]. As such basic Anderson localization [3] phenomena, Anderson's orthogonality catastrophe [4] or Kondo physics [5] might be addressed. In this context interest sparked in quantum degenerate mixtures of bosonic ytterbium (Yb) and fermionic lithium (Li) as a prime candidate to experimentally implement impurity systems. In addition, when forming dimers built-up of Yb and Li due to the combination of alkaline-earth-like atoms (Yb) and alkali ones (Li) spin-doublet molecules [6], building blocks of envisioned spin-lattice quantum simulators [7], can be realized. More recently the exploration of mixed-dimensional systems [8] and even topological superfluids [9] have also been proposed.

Common to all applications of an ultracold Yb–Li mixture system is a mandatory good understanding of the interspecies interactions. Even six years after the first successful demonstration of quantum degenerate mixtures of bosonic ytterbium (Yb) and fermionic lithium (Li) [10, 11] both a theoretical treatment of basic collisional properties in the Yb–Li mixture system and their experimental determination remain a challenging topic. In this respect important steps have been taken since the first experimental realizations. While initially only the absolute value of the interspecies ground state scattering length could be determined [10, 11] recent efforts could also confirm the interaction to be repulsive [12]. After it was shown in a first theoretical treatment that the Yb–Li ground state system probably does not support broad enough Feshbach resonances [13] that are easily exploited experimentally [14] a later work provided hints at possibly usable Feshbach resonances involving the metastable $^3P_2$ state of Yb and the ground state of Li [15]. It also recognized the importance of the anisotropy induced spin dependence in the involved interspecies interactions. Those calculations have been further pursued in later works [16, 17] and first experimental results [18, 19] followed.

In the research detailed in the present paper we study inelastic collisional properties between localized $^{174}Yb\,(^3P_2)$ atoms immersed in a Fermi sea of ^6Li. We employ a species specific, three-dimensional (3D) optical lattice and

Figure 1. (a) Principle of the experimental method. In an optical lattice (solid line) operating at wavelength $\lambda_L = 532$ nm and depth 15 E_R^{Yb} the Yb atoms (green dots) form a Mott insulator structure and are localized. For clarity only lattice sites with occupation numbers $n = 1$ and 2 are shown. In the experiment the 507 nm excitation light is tuned to only excite singly occupied lattice sites to the desired $^3P_2$ state. Li atoms (red) only experience a small density modulation in the corresponding shallow optical lattice (dashed line) at 0.7 E_R^{Li} and are delocalized. (b) Basic level structure of Yb of relevance to the experiment. The transitions for imaging and removal of ground state Yb atoms (399 nm, blue), for excitation to the $^3P_2$ state (507 nm, green) and repumping to the ground state (649 and 770 nm, red) together with their respective natural linewidths are indicated.

control the internal states of Yb by using selective excitation and those of Li by means of optical pumping. This allows for the first time a systematic study of the spin dependence in collisions between two-electron atoms in the metastable $^3P_2$ state and alkali atoms in the ground state. In previous experiments [19] we studied the inelastic collisions between ^{174}Yb$(^3P_2, m_J = \{-2, 0\})$ and ^{6}Li in the $F = 1/2$ ground state manifold. There, we provided detailed information on the inelastic loss rate coefficients, excluded spin changing collisions as dominant processes and generally found no significant differences between collisions involving the $m_J = -2$ or the $m_J = 0$ state of Yb. In the present work we investigate the full range of Yb$(^3P_2)$ Zeeman sublevels, $m_J = -2, \ldots, +2$, and four states of Li, Li$(^2S_{1/2}, F = 1/2, m_F = \pm 1/2)$ and Li$(^2S_{1/2}, F = 3/2, m_F = \pm 3/2)$. We find nearly identical inelastic collision rates for all combinations involving Li$(F = 1/2)$ and strongly state dependent rates for collisions with Li$(F = 3/2)$ atoms that vary by more than an order of magnitude. The present work unveils another piece of information on the nature of the ultracold Yb–Li collisional system and offers further insights into anisotropy induced relaxation processes in collisions involving non-S-state atoms [20–23].

2. Experimental procedure

The experiment proceeds along the same lines as presented in [19]. Briefly, a mixture of quantum degenerate ^{174}Yb and ^{6}Li is prepared by forced evaporative cooling in a crossed optical far-off-resonance trap. Different to our previous works we introduce during the initial phase of the evaporative cooling an optical pumping step to prepare a spin-polarized Li sample in either the $F = 1/2$, $m_F = \pm 1/2$ or $F = 3/2$, $m_F = \pm 3/2$ manifold of the ground state. In the former case a 0.5 ms pulse of circularly polarized light resonant to the Li $F = 1/2 \rightarrow F' = 1/2$ D1-line transition together with light resonant to the Li $F = 3/2 \rightarrow F' = 5/2$ D2-line transition is applied. In the latter case light on the D1 $(F = 3/2 \rightarrow F' = 3/2)$-line and D2 $(F = 1/2 \rightarrow F' = 3/2)$-line is used. By a suitable choice of a homogeneous magnetic bias field we can thus prepare a spin-polarized Li sample in any of the four states given above. The purity of the sample is verified by standard time-of-flight absorption imaging where the atoms expand for 1.2 ms in a strong magnetic field gradient and found to be above 90%. Care is taken to maintain a sufficiently strong bias field during the remainder of the experimental sequence of about 7 G not to lose the state of polarization. We choose the parameters of the experiment such as to typically obtain a Bose–Einstein condensate of 10×10^4 Yb atoms and a Fermi degenerate gas of 3×10^4 spin-polarized Li atoms. The temperature of Li is $T_{Li} \approx 300$ nK and $T_{Li}/T_F \approx 0.2$, where T_F is the Fermi temperature.

We then proceed to adiabatically load the quantum degenerate mixture into a 3D optical lattice with wavelength $\lambda_L = 532$ nm and depth 15 E_R^{Yb}, with E_R^{Yb} being the recoil energy of Yb in the lattice, where Yb forms a Mott insulating state [1, 19], see figure 1(a). In the same configuration the corresponding lattice depth for Li is 0.7 E_R^{Li}, where E_R^{Li} is the Li recoil energy. The sign of the polarizability of Li at λ_L is negative and the lattice sites of Yb and Li alternate. As in our previous experiment spatial overlap between the two atomic clouds is enhanced by use of a gravitational sag compensation beam that is applied while the lattice is ramped up within 200 ms to its target power. The final separation between the Yb and Li cloud center-of-mass positions is about

3.5 μm. Additionally, we adjust our magnetic bias field to 200 mG during the first 100 ms of the lattice ramp and we verified that the spin polarization of Li is maintained during this change. The bias field lifts the degeneracy of the Yb(^{3}P$_2$) Zeeman states and a resonant laser pulse of wavelength 507 nm and duration 0.5 ms excites a small fraction of the Yb atoms to the desired m_J Zeeman state. Usage of the ultranarrow transition connecting the ^{1}S$_0$ to the metastable ^{3}P$_2$ state, see figure 1(b), also allows us to selectively only excite Yb atoms in singly occupied lattice sites [19], thus suppressing inelastic decay from collisions with other Yb(^{3}P$_2$) and Yb(^{1}S$_0$) atoms [24]. During the 0.5 ms excitation time the excitation laser frequency is linearly ramped from -4 to $+4$ kHz around the resonance condition to ensure stable excitation even with slight magnetic field noise due to background magnetic field changes in the laboratory. The Zeeman splitting is 2.1 MHz G^{-1} $\times$ h $\times$ m_J, where h is the Planck constant. The intensity of the excitation light is chosen such as to excite about 2×10^3–3×10^3 atoms to the ^{3}P$_2$ state, corresponding to about 10% of the total number of Li atoms. This ensures that the excited Yb atoms can be considered to be immersed in a Fermi sea of Li atoms, i.e. the number of Li atoms can be considered as constant during the remainder of the experiment. Remaining ground state Yb atoms are removed within 0.3 ms by application of light at 399 nm resonant to the strong ^{1}S$_0 \rightarrow ^1$P$_1$ transition. This removal process ensures that also for magnetically sensitive states with $m_J \neq 0$, where spurious excitation in lattice sites with higher occupation numbers due to magnetic field fluctuations is possible, a clean sample of strictly singly occupied Yb(^{3}P$_2$) lattice sites is prepared. After a variable holding time an identical 399 nm cleaning pulse is applied and the remaining ^{3}P$_2$ atoms are repumped to the ground state where they are recaptured by a magneto-optical trap operating also on the ^{1}S$_0 \rightarrow ^1$P$_1$ transition for fluorescence imaging detection (see [19] for details). The experimental signal is thus the number of repumped Yb(^{3}P$_2$) atoms that remain in the optical lattice after the holding time. By virtue of the second cleaning pulse we are sensitive to all possible Yb(^{3}P$_2$) decay channels and measure the actual number of metastable atoms remaining after the holding time. For Yb atoms in the ^{1}S$_0$ state its depth is $15\ E_R^{Yb} = 2.9 \mu$K k_B and is for ^{3}P$_2$ excited state atoms a factor 1–1.4 deeper, depending on the m_J state.

3. Results

We systematically measure the inelastic Yb(^{3}P$_2$)-Li collisional properties for all combinations of available ^{3}P$_2$ Zeeman states, $m_J = -2, \ldots, +2$, and accessible Li ground states, $F = 1/2$, $m_F = \pm 1/2$ and $F = 3/2$, $m_F = \pm 3/2$. For each combination of collisional partners we record the decay of Yb(^{3}P$_2$) atoms by repeating the experiment several times at various holding times. Typically about 15 different holding times suitable for the observed speed of decay are chosen and at each holding time 5 (10) datapoints are taken for $|m_J| < 2$ ($|m_J| = 2$) states. More datapoints are taken for measurements involving $|m_J| = 2$ states as due to the high magnetic field sensitivity of those states, 4.2 MHz G^{-1}, data quality is reduced by inevitable magnetic field noise. Two typically obtained decay curves are shown in figure 2. The recorded decay behavior can be divided into two regimes. An initial relatively fast decay is followed by notably slower dynamics. We attribute the qualitative change to a transition from a Yb(^{3}P$_2$)-Li inelastic collisional dominated decay to a mixed dynamics where both interspecies collisions and losses due to collisions with thermal atoms and background gas are of importance.
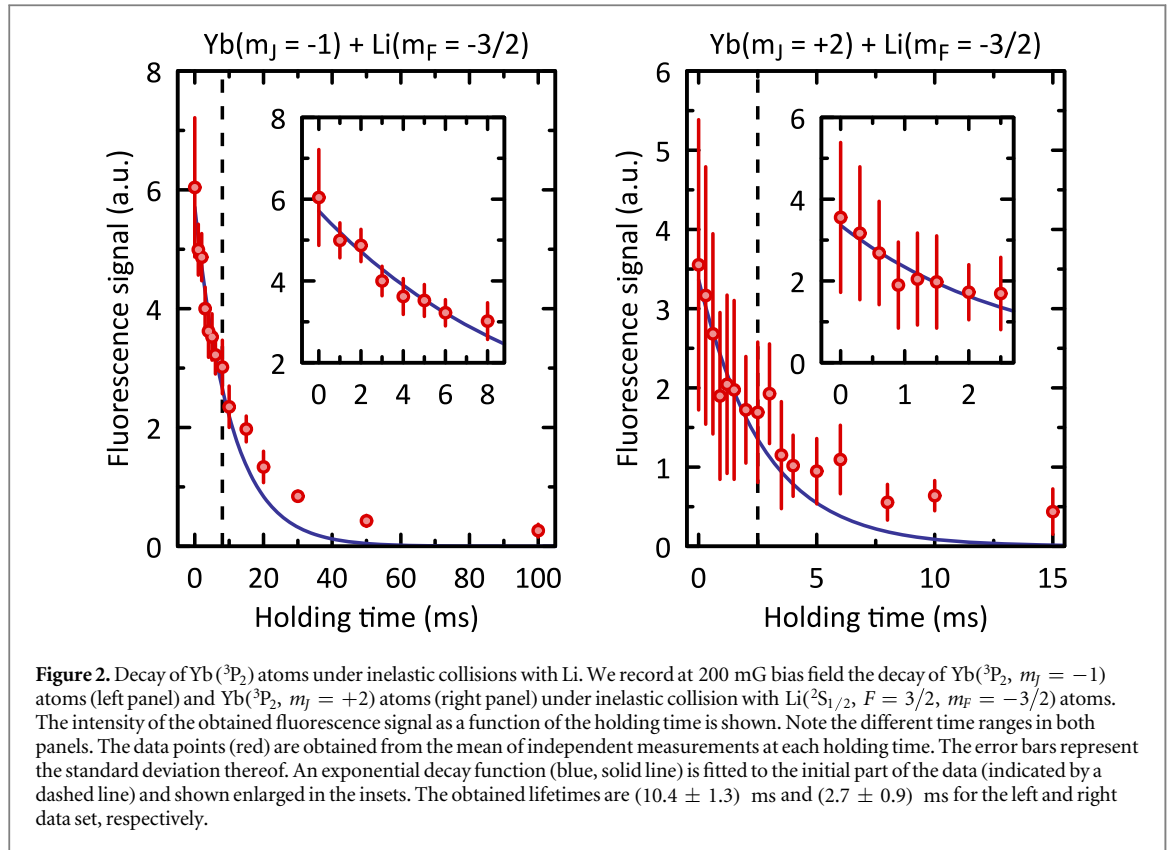
The observed decay is attributed to be mostly caused by inelastic collisions with Li atoms and to a minor extent due to collisions with background gas atoms. Collisions between two Yb(^{3}P$_2$) atoms are suppressed as their mobility is strongly reduced by the deep optical lattice. This motivates a decay model [19] for the Yb density, n_{Yb},

$$\dot{n}_{Yb}(\mathbf{r}, t) = -\alpha\, n_{Yb}(\mathbf{r}, t) - \beta\, \xi\, n_{Li}(\mathbf{r}) n_{Yb}(\mathbf{r}, t), \tag{1}$$

where α is the one-body loss rate and β the Yb(^{3}P$_2$)-Li inelastic loss coefficient. The slight modulation of the Li density n_{Li} by the optical lattice is accounted for by the density correction factor ξ. The correction factor is determined by the overlap of the Yb Wannier state and the Li Bloch state at the respective lattice depths. While the lattice depths depend on the Zeeman state dependent polarizabilities the overlap integral only weakly changes [19]. Throughout the current work a constant value of $\xi = 0.65 \pm 0.03$ is adopted. Considering the strong imbalance in the number of Li and Yb(^{3}P$_2$) atoms the density $n_{Li}(\mathbf{r})$ is taken to be constant in time. The one-body loss rate α cumulatively describes loss of Yb(^{3}P$_2$) atoms by spontaneous decay and by inelastic collisions with background gas atoms. It is determined by independent measurements in which the Li atoms have been removed from the sample by a light pulse resonant to the Li D2 line. We typically observe $\alpha^{-1} = (850 \pm 300)$ ms. The complete decay is then described by

$$N_{Yb}(t) = \int n_{Yb}(\mathbf{r}, 0) e^{-(\alpha + \beta \xi n_{Li}(\mathbf{r}))t}\, d^3r. \tag{2}$$

Even though it was shown that the complete experimentally observed decay can be described by equation (2) we here adopt a different approach to the analysis of the data. The initial loss of the total number of Yb(^{3}P$_2$) atoms, N_{Yb}, is accessible by spatial integration of equation (1),

Figure 2. Decay of Yb(^{3}P$_2$) atoms under inelastic collisions with Li. We record at 200 mG bias field the decay of Yb(^{3}P$_2$, $m_J = -1$) atoms (left panel) and Yb(^{3}P$_2$, $m_J = +2$) atoms (right panel) under inelastic collision with Li(^{2}S$_{1/2}$, $F = 3/2$, $m_F = -3/2$) atoms. The intensity of the obtained fluorescence signal as a function of the holding time is shown. Note the different time ranges in both panels. The data points (red) are obtained from the mean of independent measurements at each holding time. The error bars represent the standard deviation thereof. An exponential decay function (blue, solid line) is fitted to the initial part of the data (indicated by a dashed line) and shown enlarged in the insets. The obtained lifetimes are (10.4 ± 1.3) ms and (2.7 ± 0.9) ms for the left and right data set, respectively.

$$\dot{N}_{\text{Yb}}(t=0) = -\alpha\, N_{\text{Yb}}(t=0) - \beta\, \xi \int n_{\text{Li}}(\mathbf{r})\, n_{\text{Yb}}(\mathbf{r},\, 0)\, \mathrm{d}^3 r. \tag{3}$$

For short holding times the loss of Yb(^{3}P$_2$) atoms is further excellently described by an exponential decay behavior. Accordingly, we describe the initial decay of the data by

$$N_{\text{Yb}}^{\text{expt}}(t) = N_{\text{Yb}}(0)\, \mathrm{e}^{-t/\tau_{\text{expt}}}. \tag{4}$$

Comparison of this expression to equation (3) at $t = 0$ then gives access to the inelastic loss rate

$$\beta = \frac{N_{\text{Yb}}(0)}{\xi\, X}\left(\frac{1}{\tau_{\text{expt}}} - \alpha\right), \tag{5}$$

where we have introduced the overlap integral $X = \int n_{\text{Li}}(\mathbf{r})\, n_{\text{Yb}}(\mathbf{r},\, 0)\, \mathrm{d}^3 r$. This allows for a precise, stable and numerically fast analysis of data even under the influence of experimental noise, as illustrated in figure 2.

Special care is taken for a sound treatment of the statistical and systematic errors in the data analysis. This necessity stems in particular from the pronounced sensitivity of the Yb(^{3}P$_2$, $m_J = \pm 2$) states to magnetic noise. First, in a bootstrap approach the initial 5–10 ms of available data of each set is randomly resampled. That is, for each holding time a number of points is randomly drawn from the set of experimental data so that a new realization is obtained with the same number of data points as in the original set at each time step, that is a single point is allowed to be drawn more than once. This realization is then fitted by equation (4) and the complete resampling sequence is repeated 2000 times. Thus determined probability distribution function (PDF) of lifetimes τ_{expt} then serves as input to a second step in which equation (5) is solved, again 2000 times, where in each case new representative values for each parameter are randomly drawn from a given PDF. The obtained PDF of inelastic loss coefficients is then expressed in terms of an cumulative distribution function where the quantile at 50.0%, i.e. the median, is taken as best estimate and the quantiles at 15.9% and 84.1% serve as bounds for a 68.3%, i.e. a 1-σ, confidence interval. The assumed statistical and systematic errors are listed in table 1.

The obtained inelastic collision rates are summarized in figure 3. Two distinct and different behaviors are observed: in experiments with Li($F = 1/2$) as collisional partner the inelastic collision rate is constant at about 4×10^{-11} cm^3 s^{-1}. On the contrary, in inelastic collisions with Li($F = 3/2$) a strong, systematic dependence on the choice of m_J for Yb and m_F for Li is found. Inelastic collision rates vary between roughly 1×10^{-11} and 40×10^{-11} cm^3 s^{-1}. This is the first time that a dependence of the collisional dynamics between metastable state two-electron atoms and the ground state of alkali-atoms on the spin states of both species is confirmed experimentally and poses the main result of this work. The symmetry of the discovered spin dependence is striking. Nearly equally high inelastic collision rates are found for Yb(^{3}P$_2$, $m_J = \mp 2$)-Li($F = 3/2$, $m_F = \pm 3/2$)

Table 1. Statistical and systematic errors accounted for in the data analysis. The relative vertical distance between the Yb and Li atom cloud due to gravitational sag is denoted by δ_z, possible relative cloud position offsets in horizontal direction are $\delta_{\{x,y\}}$. The three offsets contribute to the overlap integral X.

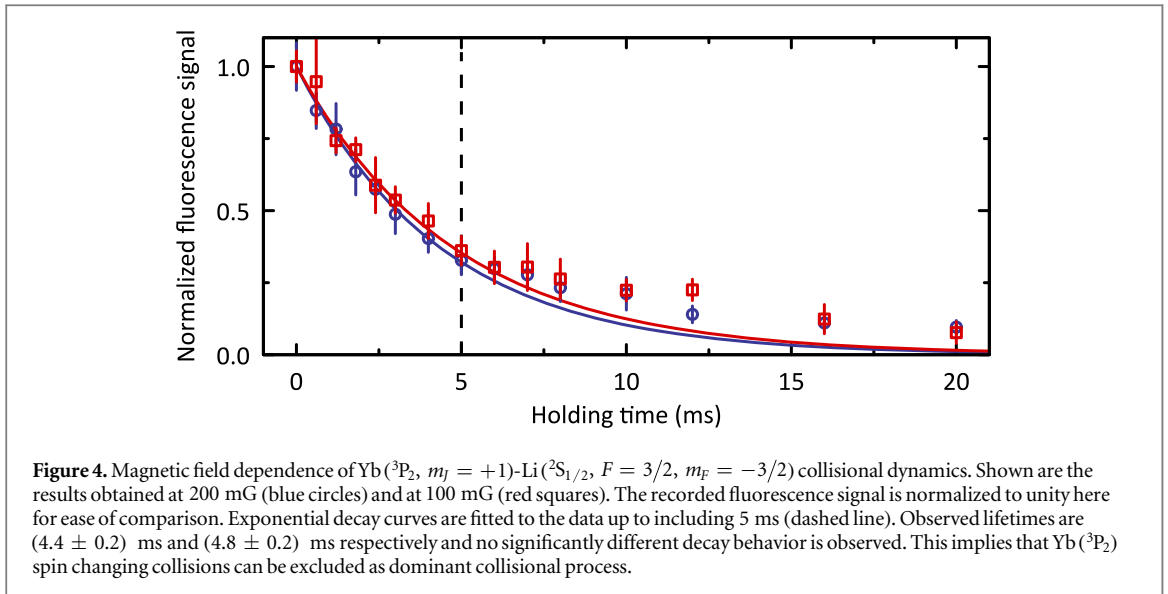| Parameter	Error type	Assumed distribution
τ	Statistic	Determined by fits to experimental data
α^{-1}	Statistic	Normal distribution, σ from fit to data
$N_{Yb}(0)$	Statistic	Normal distribution, $\sigma = 0.3\, N_{Yb}(0)$
N_{Li}	Statistic	Normal distribution, $\sigma = 0.3\, N_{Li}$
ξ	Systematic	Uniform distribution between [0.62, 0.68]
δ_z	Systematic	Uniform distribution between [2.5, 4.5] μm
δ_x, δ_y	Systematic	Uniform distribution between $[-0.5, +0.5]$ μm
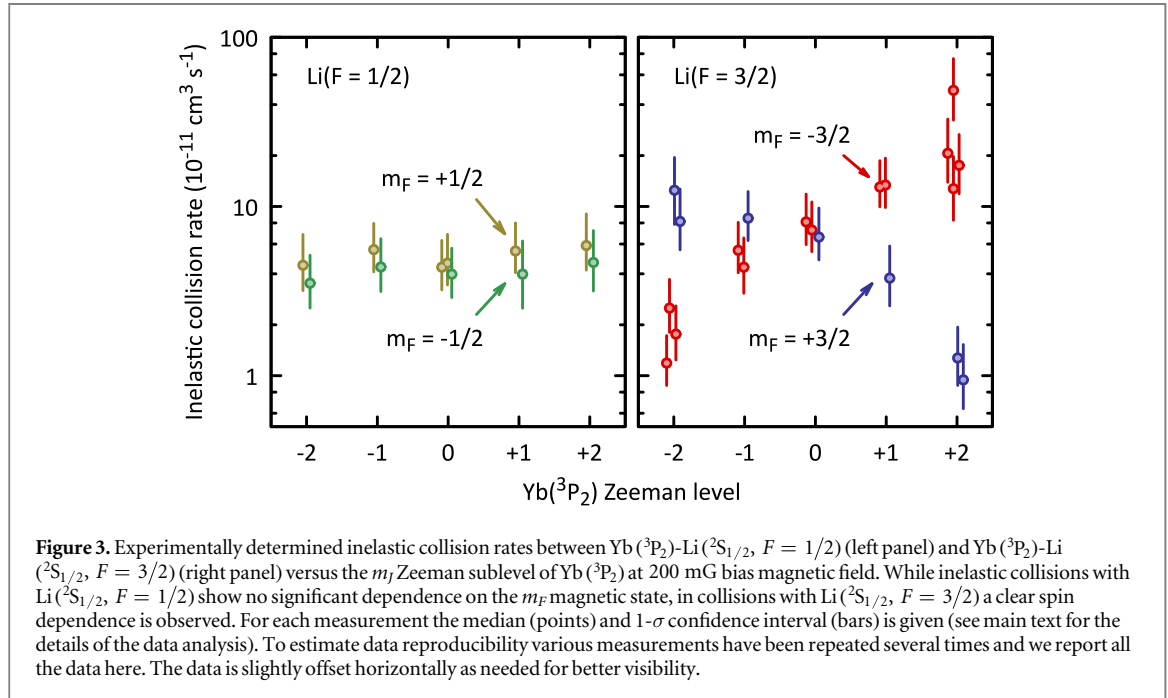
Figure 3. Experimentally determined inelastic collision rates between Yb($^3P_2$)-Li($^2S_{1/2}$, $F = 1/2$) (left panel) and Yb($^3P_2$)-Li ($^2S_{1/2}$, $F = 3/2$) (right panel) versus the m_J Zeeman sublevel of Yb($^3P_2$) at 200 mG bias magnetic field. While inelastic collisions with Li($^2S_{1/2}$, $F = 1/2$) show no significant dependence on the m_F magnetic state, in collisions with Li($^2S_{1/2}$, $F = 3/2$) a clear spin dependence is observed. For each measurement the median (points) and 1-σ confidence interval (bars) is given (see main text for the details of the data analysis). To estimate data reproducibility various measurements have been repeated several times and we report all the data here. The data is slightly offset horizontally as needed for better visibility.

processes and nearly equally low rates are seen for Yb($^3P_2$, $m_J = \pm 2$)-Li($F = 3/2$, $m_F = \pm 3/2$) stretched state collisions. In the intermediate regime, where $m_J = 0$, inelastic rates comparable to processes including Li($F = 1/2$) are found.

4. Discussion

First, we want to shed some light on the possible inelastic decay channels of importance for the collisional processes at hand. One distinguishes between (i) spin changing, (ii) fine-structure changing, (iii) hyperfine-structure changing and (iv) principal quantum number changing collisions. Spin changing collisions are to be understood as processes where m_J or m_F change, fine-structure changes imply a decay Yb($^3P_2$) $\rightarrow$ Yb($^3P_1$ or $^3P_0$), hyperfine structure changes account for Li($F = 3/2 \rightarrow 1/2$) processes and principal quantum number changes indicate a direct Yb($^3P_2$) $\rightarrow$ Yb($^1S_0$) decay. In inelastic collisions between Yb and Li about $m_{Li}/(m_{Yb} + m_{Li}) \approx 3\%$, where $m_{Yb,Li}$ denotes masses, of the released energy is transferred onto Yb. As stated before our optical lattice has for Yb a depth of at least 2.9 μK k_B. This is to be compared to the energy gain of Yb($^3P_2$) atoms in a collisional process with $m_J \mapsto m_J - 1$ which is 0.6 μK k_B at 200 mG considering the Yb–Li kinematic factor 0.03. Thus at least in $m_J = +2 \mapsto -2$ processes an energy gain of about 2.4 μK k_B might lead to the onset of increased particle loss from the optical lattice. This could partially explain the enhanced inelastic loss rate observed in Yb($^3P_2$, $m_J = +2$)-Li($^2S_{1/2}$, $F = 3/2$, $m_F = -3/2$) collisions. To exclude such a possibility in this situation the experiment is repeated at a reduced bias field of 100 mG and a comparison of both decay dynamics is shown in figure 4. No significant differences that might hint at different loss mechanisms are observed. This is in line with earlier reports of negligible spin flip processes at low magnetic fields in collisions with Li($^2S_{1/2}$, $F = 1/2$) atoms [18, 19]. Also, the observation of strong inelastic losses in Yb($^3P_2$, $m_J = -2$)-Li ($F = 3/2$, $m_F = 3/2$) collisions, where exothermic spin changes of Yb are not possible, leads to the same

Figure 4. Magnetic field dependence of Yb($^3P_2$, $m_J = +1$)-Li($^2S_{1/2}$, $F = 3/2$, $m_F = -3/2$) collisional dynamics. Shown are the results obtained at 200 mG (blue circles) and at 100 mG (red squares). The recorded fluorescence signal is normalized to unity here for ease of comparison. Exponential decay curves are fitted to the data up to including 5 ms (dashed line). Observed lifetimes are (4.4 ± 0.2) ms and (4.8 ± 0.2) ms respectively and no significantly different decay behavior is observed. This implies that Yb($^3P_2$) spin changing collisions can be excluded as dominant collisional process.

conclusion. Note that for Li a change $m_F \mapsto m_F - 1$ only heats up Yb by $0.27 \mu K$ and does not cause trap loss at both magnetic fields considered. However, a hyperfine-structure changing event will heat Yb by 330 μK and surely lead to loss of Yb.

We now focus on the magnetic sublevel dependence of the observed inelastic collision rates (see figure 3). In short, while constant relaxation rates are seen with Li($^2S_{1/2}$, $F = 1/2$) as collisional partner, for Li($^2S_{1/2}$, $F = 3/2$) suppression of Zeeman relaxation [22, 23] in the stretched state system and systematically increased inelastic collision rates for other Yb($^3P_2$) Zeeman sublevels are found. While a complete description of the system Hamiltonian can be found for example in [15] for the following discussion it will be sufficient to only consider $\hat{U}(R)$, the interspecies interaction operator as function of the relative distance R between the Yb($^3P_2$) and Li atoms. The interaction produces four molecular states ($^2\Sigma^+$, $^2\Pi$, $^4\Sigma^+$ and $^4\Pi$) that in the limit $R \rightarrow \infty$ dissociate to the Yb(^3P)-Li($^2S_{1/2}$) states. The four potential curves are shown in [15, 16] to differ significantly at intermediate distances and, accordingly, considerable Zeeman relaxation processes are expected [25]. Therefore, the interplay between anisotropic interaction induced decay and total spin conserving processes, where the latter is the usual condition for alkali dimers, should lead to spin dependent and enhanced relaxation mechanism. Indeed, our inelastic collision rates are three to four orders of magnitude larger than those reported for, e.g., Ti($^3F_2$)-He collisions [26] where anisotropy induced effects are suppressed due to screening by outer $4s$ orbitals. Lack of such a screening mechanism in the Yb($^3P_2$)-Li system is generally confirmed by our data.

The interspecies interaction conserves $M_{tot} = m_{J_{Yb}} + m_{F_{Li}} + m_l$, the sum of the Yb and Li angular momentum projections onto the axis of the applied magnetic field and m_l, the projection of the collisional channel angular momentum [15, 16]. Considering the case $m_l = 0$ conservation of M_{tot} leads to a lack of inelastic decay channels for collisions in a stretched state configuration. Even though a complete absence of inelastic decay is not observed in our experimental data a strong suppression is revealed. More precisely, the observed losses are due to the anisotropy in $\hat{U}(R)$. In [22] the concept of internal and external anisotropy in collisions with non-S-state atoms was introduced as leading and higher order terms, respectively, in a tensorial expansion of the Born–Oppenheimer potential. The internal anisotropy part of $\hat{U}$ does not couple electronic angular momentum to the rotational angular momentum of the nuclei and drives transitions $|j_{Yb}, m_{j_{Yb}}\rangle |f_{Li}, m_{f_{Li}}\rangle \rightarrow |j'_{Yb}, m_{j_{Yb}} + \Delta m\rangle |f'_{Li}, m_{f_{Li}} - \Delta m\rangle$. Here, j_{Yb} and f_{Li} denote the atomic angular momenta of the respective atomic species, their projections being expressed as $m_{j_{Yb}}$ and $m_{f_{Li}}$. Internal anisotropy preserves total electronic angular momentum and its projection. This implies that internal anisotropy cannot drive transitions in stretched state collisions. In contrast to this, the external anisotropy part couples to the rotational momentum of the nuclei and causes transitions $|j_{Yb}, m_{j_{Yb}}\rangle |f_{Li}, m_{f_{Li}}\rangle \rightarrow |j'_{Yb}, m_{j'_{Yb}}\rangle |f'_{Li}, m_{f'_{Li}}\rangle$. It does not preserve electronic angular momentum and therefore allows for transitions in stretched state collisions. Our stretched state results ($M_{tot} = \pm 7/2$) estimate in very good agreement with the theoretical result [15] the external anisotropy induced inelastic collision rate to about 1×10^{-11} cm^3 s^{-1}. In contrast, in non-stretched state collisions not only external anisotropy but also internal anisotropy leads to relaxation effects. The strong impact of the internal anisotropy is underlined by the more than tenfold enhanced inelastic collision rates observed for $M_{tot} = \pm 1/2$ that approach the predicted universal loss rate [15, 27] at 2.9×10^{-10} cm^3 s^{-1} indicative of complete loss at short range. As demonstrated in [28], strong deviations from the universal model can lead to pronounced fluctuations of the collisional cross-sections.

Turning our attention to inelastic processes involving $Li(F = 1/2)$ states (see figure 3, left) a structureless behavior is found. In all spin combinations the inelastic collision rate is about 4×10^{-11} cm^3 s^{-1}, roughly equal to the mean behavior observed with $Li(F = 3/2)$ for $1/2 < |M_{tot}| < 7/2$. The reason for this stark difference is not clear and no systematic theoretical investigation of this particular case has yet been reported. In particular the role of possible $Li(F = 3/2) \rightarrow Li(F = 1/2)$ relaxation processes is unknown. Due to the large energy gain in such a hyperfine-level changing collision the involved Li atom is surely lost from our trap and cannot be distinguished from a Li m_F changing event in the current experiment.

5. Conclusions and outlook

Investigating state selectively excited $Yb(^3P_2)$ in a deep optical lattice embedded in a sea of spin polarized Li we reported the interspecies inelastic collision rates for different spin configurations of the constituents at low magnetic fields. Of particular interest was the systematic dependence of the $Yb(^3P_2)$-$Li(F = 3/2)$ inelastic collision rate on $|M_{tot}|$ where suppressed relaxation for the stretched states, $|M_{tot}| = 7/2$, and more than tenfold increased loss rates were found for $|M_{tot}| = 1/2$. While we could demonstrate those results to be consistent with the ongoing research on collisions involving non-S-state atoms a detailed understanding, in particular of the $Yb(^3P_2)$-$Li(F = 1/2)$ collisional process, is as of yet missing. The presented data should thus stimulate new theoretical efforts for a better grasp on the details of the physical processes involved. At the same time the results indicate that in particular the stretched state configurations might be noteworthy candidates for future experiments dedicated to find means to tune the $Yb(^3P_2)$-Li interspecies interactions by a Feshbach resonance effect. It will now be a new challenge to take the presented results as a starting point for systematic investigations at stronger magnetic bias fields so that finally a good understanding of the $Yb(^3P_2)$-Li system might be achieved.

Acknowledgments

ORCID iDs

Florian Schäfer https://orcid.org/0000-0003-2198-0709

References

[1] Bloch I, Dalibard J and Zwerger W 2008 *Rev. Mod. Phys.* **80** 885–964
[2] Massignan P, Zaccanti M and Bruun G M 2014 *Rep. Prog. Phys.* **77** 034401
[3] Anderson P W 1958 *Phys. Rev.* **109** 1492–505
[4] Anderson P W 1967 *Phys. Rev. Lett.* **18** 1049–51
[5] Kondo J 1964 *Prog. Theor. Phys.* **32** 37–49
[6] Roy R, Shrestha R, Green A, Gupta S, Li M, Kotochigova S, Petrov A and Yuen C H 2016 *Phys. Rev. A* **94** 033413
[7] Micheli A, Brennen G K and Zoller P 2006 *Nat. Phys.* **2** 341–7
[8] Nishida Y 2010 *Phys. Rev. A* **82** 011605
[9] Caracanhas M A, Schreck F and Smith C M 2017 *New J. Phys.* accepted manuscript (https://doi.org/10.1088/1367-2630/aa8e56)
[10] Hansen A H, Khramov A, Dowd W H, Jamison A O, Ivanov V V and Gupta S 2011 *Phys. Rev. A* **84** 011606
[11] Hara H, Takasu Y, Yamaoka Y, Doyle J M and Takahashi Y 2011 *Phys. Rev. Lett.* **106** 205304
[12] Roy R, Green A, Bowler R and Gupta S 2017 *Phys. Rev. Lett.* **118** 055301
[13] Chin C, Grimm R, Julienne P and Tiesinga E 2010 *Rev. Mod. Phys.* **82** 1225
[14] Brue D A and Hutson J M 2012 *Phys. Rev. Lett.* **108** 043201
[15] González-Martínez M L and Hutson J M 2013 *Phys. Rev. A* **88** 020701
[16] Petrov A, Makrides C and Kotochigova S 2015 *New J. Phys.* **17** 045010
[17] Chen T, Zhang C, Li X, Qian J and Wang Y 2015 *New J. Phys.* **17** 103036
[18] Dowd W, Roy R J, Shrestha R K, Petrov A, Makrides C, Kotochigova S and Gupta S 2015 *New J. Phys.* **17** 055007
[19] Konishi H, Schäfer F, Ueda S and Takahashi Y 2016 *New J. Phys.* **18** 103009
[20] Reid R H G and Dalgarno A 1969 *Phys. Rev. Lett.* **22** 1029–30
[21] Mies F H 1973 *Phys. Rev. A* **7** 942–57
[22] Krems R V, Groenenboom G C and Dalgarno A 2004 *J. Phys. Chem. A* **108** 8941–8
[23] Hancox C I, Doret S C, Hummon M T, Luo L and Doyle J M 2004 *Nature* **431** 281–4
[24] Uetake S, Murakami R, Doyle J M and Takahashi Y 2012 *Phys. Rev.* **86** 032712
[25] Krems R V, Kos J, Rode M F, Szczniak M M, Chaaasiski G and Dalgarno A 2005 *Phys. Rev. Lett.* **94** 013202
[26] Hancox C I, Doret S C, Hummon M T, Krems R V and Doyle J M 2005 *Phys. Rev. Lett.* **94** 013201
[27] Idziaszek Z and Julienne P S 2010 *Phys. Rev. Lett.* **104** 113202
[28] Frye M D, Julienne P S and Hutson J M 2015 *New J. Phys.* **17** 045019